Journal of the European Ceramic Society xxx (xxxx) xxx

Contents lists available at ScienceDirect

Journal of the European Ceramic Society

journal homepage: www.elsevier.com/locate/jeurceramsoc

Relationship between Rattling Mg^{2+} ions and anomalous microwave dielectric behavior in $Ca_{3-x}Mg_{1+x}LiV_3O_{12}$ ceramics with garnet structure

Ying Tang [a,b], Huan Li [a], Jie Li [a,b,*], Weishuang Fang [a], Yang Yang [a], Zhiyuan Zhang [a], Liang Fang [a,b,*]

[a] Guangxi Key Laboratory of Optical and Electronic Materials and Devices, College of Material Science and Engineering, Guilin University of Technology, Guilin, 541004, China

[b] Key Laboratory of New Processing Technology for Nonferrous Metal & Materials, Ministry of Education, Guilin University of Technology, Guilin, 541004, China

ARTICLE INFO

Keywords:
Garnet
Low permittivity
"rattling" effect
LTCC

ABSTRACT

$Ca_{3-x}Mg_{1+x}LiV_3O_{12}$ ($0 \leq x \leq 1$) ceramics with cubic-garnet-structure were synthesized by the solid-phase reaction. The replacement of Ca^{2+} with the smaller Mg^{2+} exerted an increasingly strong "rattling" effect at the A-site of $Ca_{3-x}Mg_{1+x}LiV_3O_{12}$. With increased Mg^{2+}, ε_r increased from 10.5 ± 0.1 to 15.4 ± 0.1 and ε_{corr} increased from 11.0 ± 0.1 to 16.0 ± 0.1, whereas the theoretical ε_{th} decreased from 12.0 ± 0.1 to 10.5 ± 0.1. ε_{corr} was higher than ε_{th} due to the "rattling" effect. The enhanced "rattling" effect caused τ_f to increase rapidly from –64.1 ± 1.0 ppm/°C to +267.2 ± 1.0 ppm/°C. With increased x, $Q \times f$ decreased from 74,700 ± 500 GHz to 15,370 ± 500 GHz, due to the decreased packing fraction, increased FWHM of the A_{1g} modes, and enhanced "rattling" effect. Additionally, the chemical compatibility between $Ca_{2.75}Mg_{1.25}LiV_3O_{12}$ and Ag electrodes was confirmed, indicating this material's potential for LTCC.

1. Introduction

As mobile-communication technology develops toward high frequency and high integration, requirements are increasing for the performance of microwave dielectric ceramic materials used for communication components [1]. Low permittivity (ε_r) can reduce the signal-transmission-time and mutual-coupling-loss in the components. A high Q factor can also provide good frequency-control accuracy and high passband-edge signal-frequency response steepness. A near-zero temperature coefficient of resonant frequency (τ_f) can further achieve high reliability and stability of microwave equipment [2–5]. Moreover, microwave ceramics with low sintering temperature (< 961 °C, i.e, the melting point of Ag) are required for low-temperature co-fired ceramic (LTCC) technology [6].

Vanadium-based compounds with garnet structure, such as $LiCa_3MgV_3O_{12}$ [7], $LiCa_3ZnV_3O_{12}$ [8], $AgCa_2Mg_2V_3O_{12}$ [9], $Ca_5Ni_2Mg_2V_6O_{24}$ [10] and $AgPb_2B_2V_3O_{12}$ (B = Mg, Zn) [11], are gaining considerable attention in material research due to their low ε_r, high $Q \times f$ and low-firing temperature. However, these vanadium-based garnet compounds are similar to most other low-ε_r microwave dielectric ceramics, which exhibit largely negative τ_f values. Only $LiCa_2Mg_2V_3O_{12}$ and $KCa_2Mg_2V_3O_{12}$ are unique microwave dielectric materials with a rare largely positive τ_f. Their microwave dielectric properties are $\varepsilon_r \sim 9.8$, $Q \times f \sim 24{,}900$ GHz, and $\tau_f \sim +259.2$ ppm/°C for $LiCa_2Mg_2V_3O_{12}$, as well as $\varepsilon_r \sim 10$, $Q \times f \sim 30{,}330$ GHz, and $\tau_f \sim +190.9$ ppm/°C for $KCa_2Mg_2V_3O_{12}$ [12]. Meanwhile, the reason for the largely positive τ_f in the above two vanadate compounds is unclear. Our group has previously reported that Ge-based garnet $Mg_3Y_2Ge_3O_{12}$ with mixed distribution of Mg^{2+}/Y^{3+} at the A-site has an abnormal positive τ_f of +120.5 ppm/°C, which causes the "rattling" effect on the A-site. This effect yields measured ε_r higher than the theoretical ε_{th} and a considerably lower $Q \times f$ [13]. Similar "rattling" cations also exist at the A-site of $(Ba,Sr)Ge_4O_9$, and replacing Ba with Sr can adjust the "rattling" effect. Thus, the negative τ_f of $BaGe_4O_9$ (–44.2 ppm/°C) can be adjusted to near-zero (–11.7 ppm/°C), and a high quality factor can be maintained [14]. The "rattling" cation effect was first described by Dunitz and Orgel as "the central cation at the center of the octahedron gradually becoming loose, forming the off-center displacement characteristics of ferroelectric and antiferroelectric materials" with decreased size of the central cation in the octahedron [15]. The polyhedra can be altered to

* Corresponding authors at: Guangxi Key Laboratory of Optical and Electronic Materials and Devices, College of Material Science and Engineering, Guilin University of Technology, Guilin, 541004, China.

E-mail addresses: jielee@glut.edu.cn (J. Li), fanglianggl001@aliyun.com (L. Fang).

https://doi.org/10.1016/j.jeurceramsoc.2021.08.007
Received 7 June 2021; Received in revised form 5 August 2021; Accepted 6 August 2021
Available online 11 August 2021

accommodate small cations by the movement of cations and/or anions, leading to polyhedral distortion. When the motion of cations and/or anions is restricted by crystal symmetry, such as in $(Ca_{1-0.3x}La_{0.2x})[(Mg_{1/3}Ta_{2/3})_{1-x}Ti_x]O_3$ and other complex perovskite ceramics, larger than normal bond distances and/or thermal motions may occur, resulting in abnormally large polarizabilities [16–18]. Bond valence can provide an indication of the "rattling" of a cation in its site [19].

In $LiCa_3MgV_3O_{12}$, the Ca^{2+} cations occupy the A-site to form a $[CaO_8]$ dodecahedron with the Wyckoff symbol of 24*c*. Mg^{2+} and Li^+ cations occupy the B-site with a 16*a* position, and the V^{5+} cations occupy the C-site to form a $[VO_4]$ tetrahedron with the 24*d* position [20]. Compared with $LiCa_3MgV_3O_{12}$, the crystal structure of $LiCa_2Mg_2V_3O_{12}$ comprises one Mg^{2+} and one Ca^{2+} ions occupying the A site together, and the other Mg^{2+} and Li^+ ions are located at the B-site [21]. The replacement of Ca^{2+} with the smaller Mg^{2+} may cause the "rattling" effect at the A-site of $LiCa_2Mg_2V_3O_{12}$. To verify whether a "rattling" effect existed in $LiCa_2Mg_2V_3O_{12}$, we designed herein the replacement of Ca^{2+} at A-site with different amounts of Mg^{2+} to prepare a series of $Ca_{3-x}Mg_{1+x}LiV_3O_{12}$ ($x = 0, 0.25, 0.5, 0.75, 1$) ceramics. The relationship between the "rattling" effect and microwave dielectric properties of $Ca_{3-x}Mg_{1+x}LiV_3O_{12}$ ceramics were investigated in detail by using the bond valence. The chemical compatibility of ceramics and Ag electrode for LTCC technology was also investigated.

2. Experimental procedure

Appropriate proportions of high-purity powders of $CaCO_3$(99.99 %, Aladdin), MgO (99.99 %, Aladdin), Li_2CO_3 (99.99 %, Aladdin) and NH_4VO_3 (99.99 %, Aladdin) were weighed based on the stoichiometric formulation $Ca_{3-x}Mg_{1+x}LiV_3O_{12}$ ($x = 0, 0.25, 0.5, 0.75, 1$). Before weighing, MgO powders were calcined at 900 °C for 2 h to remove water content. Then, the raw materials were mixed by ball milling for 6 h with alcohol as the medium, and the slurries were dried at 120 °C for 2 h and calcined at 700 °C for 4 h. Afterwards, the obtained powders were ball milled and dried. The dried powders were manual grinded with 5 wt.% solution of PVA as binder and pressed into cylinders (10 mm in diameter and 6 mm in thickness) at a pressure of 150 MPa. Subsequently, the pellets were heated from room temperature to 550 °C for 4 h to burn off the organic binder and then sintered at 820 °C to 900 °C for 4 h. The ceramics were polished using a Phoenix 4000 Sample Preparation System and PSA-backed polishing cloths (30 μm, 9 μm, 3 μm and 0.2 μm in sequence). The polished samples were thermally etched at 50 °C below the optimal sintering temperature for 20 min at the heating rate of 5 °C/min. Finally, the $Ca_{2.75}Mg_{1.25}LiV_3O_{12}$ ceramic were co-fired with 20 wt.% Ag powders at 880 °C for 4 h to study their compatibility.

The phase purity and crystal structures of the specimens were identified via powder X-ray diffraction (Model X'Pert PRO, PANalytical, Empyrean, Holland) using CuK_α radiation and structural Rietveld refinements were carried by Fullprof programs [22]. To observe the grain morphology of the specimens, the surface of polished and thermally etched ceramics was recorded by scanning electron microscopy (FESEM, S4800, Hitachi) and their grain sizes were measured by the linear intercept [23]. The bulk density of sintered ceramics was determined via the Archimedes' method. The room temperature Raman spectra were recorded by Raman spectrometer (DXR, Thermo Fisher Scientific, America) using a 532 nm laser in the wavenumber started from 100 cm^{-1} to 1000 cm^{-1} with a spectral resolution of 1 cm^{-1}. The ε_r and $Q \times f$ values of the ceramics were determined by the Hakki-Coleman method through the network analyzer (N5230A, Agilent, America) [24]. The τ_f values of the ceramics were measured using a temperature chamber and calculated by Formula (1):

$$\tau_f = \frac{f_{85} - f_{25}}{(85-25)f_{25}} \quad (1)$$

where, f_{85} and f_{25} represented the resonant frequencies at 85 °C and 25 °C, respectively.

3. Results and discussion

Fig. 1 demonstrates the room temperature XRD patterns of $Ca_{3-x}Mg_{1+x}LiV_3O_{12}$ ($x = 0, 0.25, 0.5, 0.75, 1$) ceramics sintered at their optimised temperature (880 °C) for 4 h. For $Ca_{3-x}Mg_{1+x}LiV_3O_{12}$ ceramics, all observed diffraction peaks could be identified with JCPDS file No. 00-24-1212, revealing that the samples crystallized into a cubic-garnet-structure with space group *Ia*-3*d*. No distinct second phase was observed in all ceramics, indicating that Mg^{2+} substituted for Ca^{2+} in $Ca_3MgLiV_3O_{12}$ to form a solid solution of $Ca_{3-x}Mg_{1+x}LiV_3O_{12}$ ceramics. As the content of Mg^{2+} increased, the main diffraction peaks of (4 2 0) slightly shifted to high angles (Fig. 1(b)), which was ascribed to the smaller ionic radius of Mg^{2+} (0.89 Å) than Ca^{2+} (1.12 Å), demonstrating decreased lattice parameter and unit cell volume.

To further investigate the influence of Mg^{2+} substituting for Ca^{2+} on microwave dielectric performances and crystal structure, the Rietveld refinements of XRD were determined using the Fullprof program. Fig. 2 (a) shows the experimental data and refined XRD patterns of $x = 0.25$ ceramic, and the others are shown in Fig. S1. The experimental data well fitted the refined patterns with the cubic-garnet-structure. Table 1 summarizes the lattice parameters, cell volume, and refined structural parameters of $Ca_{3-x}Mg_{1+x}LiV_3O_{12}$ ceramics. The Wyckoff positions, occupancy, and atomic displacement parameters are listed in Table S1. Lattice parameters slightly decreased with increased Mg^{2+} content and volume shrinkage, which corresponded to the high angle shift of the main XRD peak [25]. The A-site bond length also showed the same decreasing trend due to the ionic radius of Mg^{2+} being smaller than that of Ca^{2+}. Fig. 2(b) shows the plot of the polyhedral evolution of the prepared ceramics. For $x = 0$, the Ca^{2+} cations were at the A-site, forming a $[CaO_8]$ dodecahedron with a 24*c* site, and Mg^{2+} and Li^+ were at the B-site with a 16*a* site [20]. As the substitution of Mg^{2+} for Ca^{2+} increased from 0 to 1, the small Mg^{2+} gradually occupied the A-site of Ca^{2+}, and the percentage of Mg^{2+} at the A-site increased from 0 to 1/3, whereas the B-site was still occupied by one Mg^{2+} and one Li^+. As Barbier et al [26]. and Ganesanpotti et al [27]. revealed, normal garnets have $[A_3]\{B_2\}(C_3)O_{12}$ stoichiometry, where brackets denote the dodecahedral, octahedral, and tetrahedral coordination of cations, respectively. The cation distribution of inverse garnet is $[AB_2]\{A_2\}(C_3)O_{12}$ where brackets denote dodecahedral, octahedral, and tetrahedral sites, respectively. In particular, the dodecahedral site of inverse garnet has a mixed occupancy of A/B cations. For $x = 1$ ($Ca_2Mg_2LiV_3O_{12}$), the dodecahedral site is occupied by mixed Mg^{2+}/Ca^{2+} at 1:2 ratio, indicating that $Ca_2Mg_2LiV_3O_{12}$ has an inverse garnet structure.

Fig. 3 shows the room-temperature Raman spectra of $Ca_{3-x}Mg_{1+x}LiV_3O_{12}$ ceramics. The Raman vibrational mode is a significant parameter used to investigate the relationship between microwave dielectric

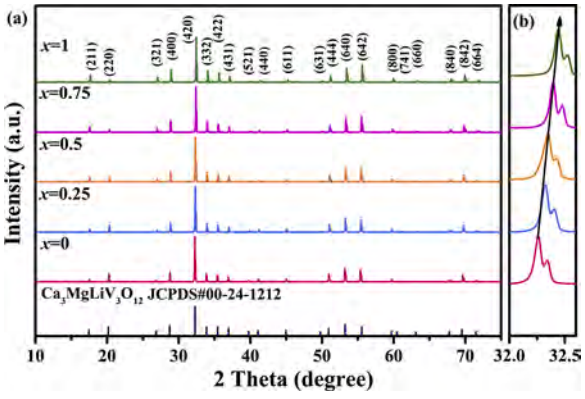

Fig. 1. XRD patterns of $Ca_{3-x}Mg_{1+x}LiV_3O_{12}$ ceramics sintered at their optimised temperature of 880 °C for 4 h.

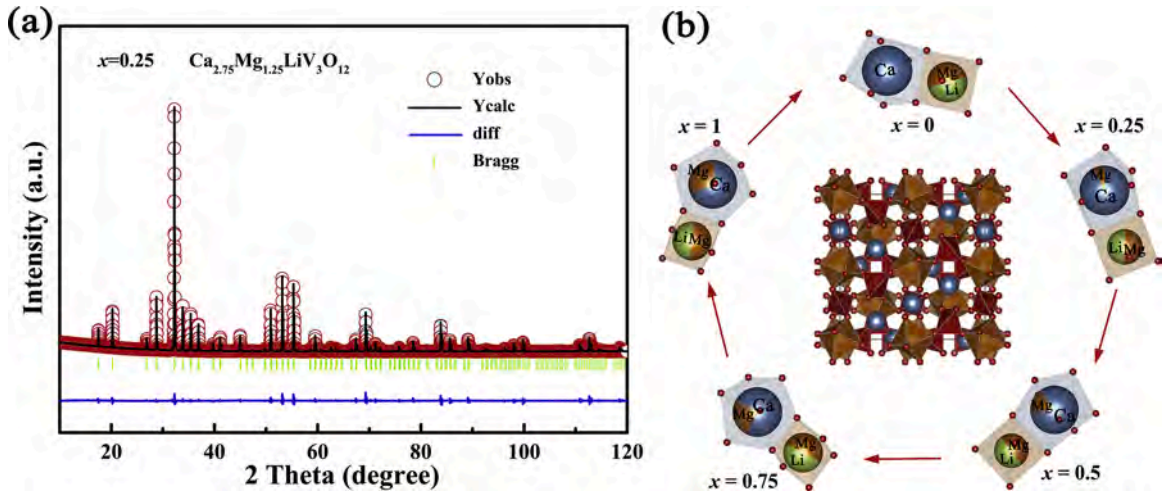

Fig. 2. (a) The XRD pattern of Rietveld refinement for $Ca_{2.75}Mg_{1.25}LiV_3O_{12}$ ceramic; (b) the polyhedral evolution of $Ca_{3-x}Mg_{1+x}LiV_3O_{12}$ ceramics.

Table 1
The lattice parameters, volume of unit cell, and Rietveld refinement parameters of $Ca_{3-x}Mg_{1+x}LiV_3O_{12}$ ceramics sintered at their optimised temperature.

x value	a (Å)	V(Å^3)	R_p (%)	R_{wp} (%)	χ^2
0	12.429(0)	1920.310(5)	2.58	3.43	4.27
0.25	12.417(9)	1914.569(0)	2.90	4.19	6.36
0.5	12.404(0)	1908.700(5)	2.42	3.12	3.55
0.75	12.389(6)	1901.876(7)	3.09	4.33	6.90
1	12.382(4)	1898.654(9)	6.62	8.75	1.59

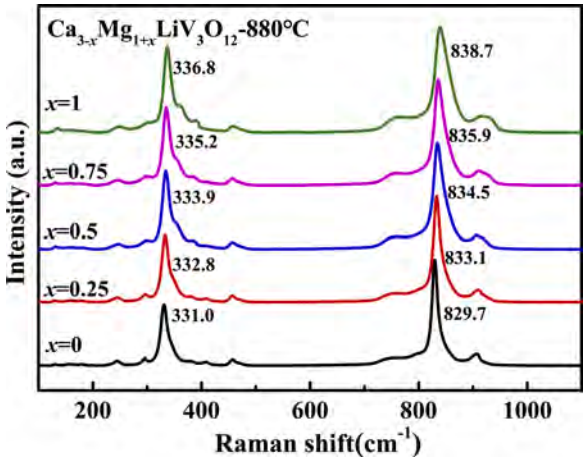

Fig. 3. The Raman spectra of $Ca_{3-x}Mg_{1+x}LiV_3O_{12}$ ceramics sintered at the optimised temperature.

performance and crystal structure [28]. According to literature, modes with the maximum intensity (~ 829.7 cm^{-1}) correspond with the stretching vibrations of the VO_4 group, denoted as A_{1g}, and linearly depend on the lattice parameter. Herein, the modes at around 331.0 cm^{-1} were assigned to the bending vibrations of VO_4 [29]. The vibrational modes shifted toward the higher-frequency side with x due to the decreased cell volume and bond length with increased substitution of Mg^{2+} for Ca^{2+}. Meanwhile, the full width at half-maxima (FWHM) for the A_{1g} modes gradually decreased, which can be used to explain the changes in microwave dielectric properties. Fig. S2 shows the deconvoluted Raman spectra of $Ca_{3-x}Mg_{1+x}LiV_3O_{12}$ (x = 0, 0.25, 0.5, 0.75, 1) sintered at 880 °C in detail.

Fig. 4 shows the surface microstructures of polished and thermally etched $Ca_{3-x}Mg_{1+x}LiV_3O_{12}$ (x = 0, 0.25, 1) ceramics sintered at their densification temperature (880 °C), and the corresponding grain size distributions. Apparently, all ceramics had a dense microstructure with typical granular particle and a clear grain boundary. With increased substitution of Mg^{2+} for Ca^{2+}, the average grain size remained stable and fluctuated around at 2.20 ± 0.08 μm.

Table 2 lists the optimized sintering temperature (S.T.), ρ_{bulk}, ρ_{rel}, ionic polarizability, and microwave dielectric properties of $Ca_{3-x}Mg_{1+x}LiV_3O_{12}$ ceramics in detail. With increased substitution of Mg^{2+} for Ca^{2+}, bulk density slightly decreased and relative density slightly increased beyond 95%. The measured ε_r monotonically increased from 10.5 ± 0.1 to 15.4 ± 0.1, whereas the calculated ε_{th} gradually increased, and so did α_{th}/V_m. $Q \times f$ decreased rapidly from 74,700 ± 500 GHz (x = 0) to 38,320 ± 500 GHz (x = 0.25) and then decreased gradually to 15,370 ± 500 GHz ((x = 1). Moreover, τ_f continuously increased in a positive direction, i.e., from the negative value of –64.1 ± 1.0 ppm/°C to the largely positive value of +267.2 ± 1.0 ppm/°C, and was close to zero (–1.6 ± 1.0 ppm/°C) at x = 0.25. The microwave dielectric properties of $\varepsilon_r \sim 11.5 \pm 0.1$, $Q \times f \sim 38{,}320 \pm 500$ GHz were also favorable.

The ε_r of the ceramics can be affected by extrinsic factors including second phase, average ionic polarisability, and relative density, as well as intrinsic factors such as lattice vibration [19,30,31]. When the relative density of single-phase $Ca_{3-x}Mg_{1+x}LiV_3O_{12}$ ceramics reached above 95 %, the effect of porosity on microwave dielectric performances was negligible. To further eliminate the effect of porosity on the ε_r of samples, the corrected permittivity ε_{corr} was calculated using Bosman and Having's equation [32]:

$$\varepsilon_{corr} = \varepsilon_r(1 + 1.5p) \quad (2)$$

where ε_{corr} and ε_r are the corrected and measured permittivity of porosity, respectively, and p is the fractional porosity. As Shannon [19] suggested, the conventional additive rules can be used to calculate the theoretical dielectric polarizability (α_{th}). Furthermore, the theoretical dielectric constant (ε_{th}) can be calculated based on the Clausius-Mossotti relationship [33].

$$\alpha_{th} = \alpha(Li^+) + (3\text{-}x)\alpha(Ca^{2+}) + (1+x)\alpha(Mg^{2+}) + 3\alpha(V^{5+}) + 12\alpha(O^{2-}) \quad (3)$$

$$\varepsilon_{th} = \frac{1 + 2b\alpha_{th}^T/V_m}{1 - b\alpha_{th}^T/V_m} \quad (4)$$

where $\alpha(Li^+) = 1.2$ Å^3, $\alpha(Ca^{2+}) = 3.16$ Å^3, $\alpha(Mg^{2+}) = 1.32$ Å^3, $\alpha(V^{5+}) = 2.92$ Å^3, and $\alpha(O^{2-}) = 2.01$ Å^3 are the ionic polarizability [19], b is a constant with a value of $4\pi/3$ and V_m is the molar volume. Fig. 5 shows the variation in ε_r, ε_{corr}, and ε_{th} with x. All ε_{corr} were higher than the

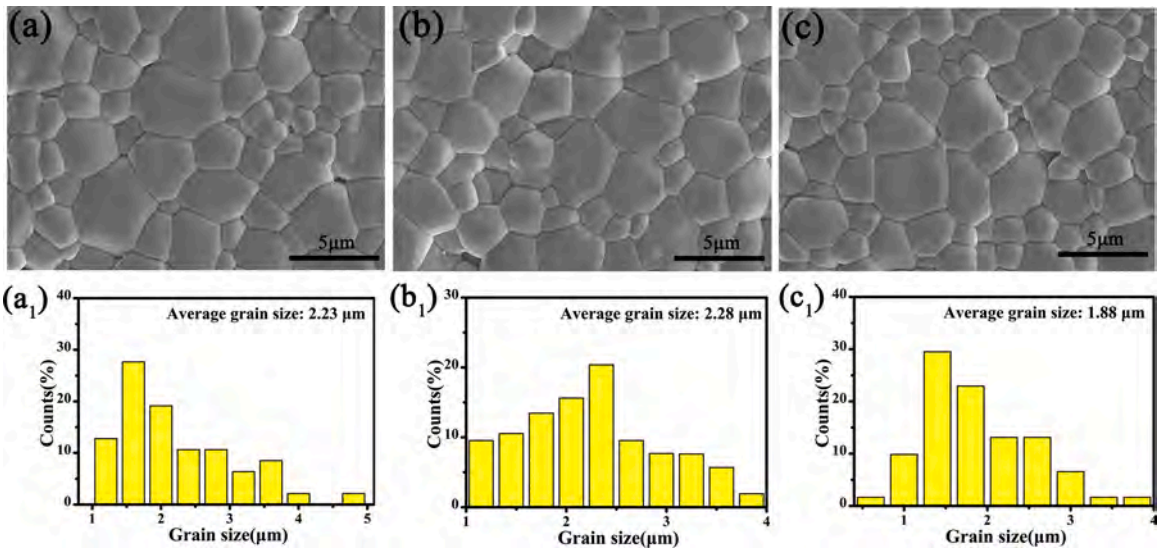

Fig. 4. (a-c) SEM photographs of the polished and thermally etched $Ca_{3-x}Mg_{1+x}LiV_3O_{12}$ ($x = 0$, 0.25, 1) ceramics sintered at optimized sintering temperature of 880 °C; (a_1-c_1) the corresponding grain size distributions.

Table 2
The optimised sintering temperatures, bulk density (ρ_{bulk}), relative density (ρ_{rel}) and microwave dielectric properties of $Ca_{3-x}Mg_{1+x}LiV_3O_{12}$ ceramics.

x	S.T. (°C)	ρ_{bulk}	ρ_{rel}	ε_r	ε_{corr}	ε_{th}	α_{th}	α_{th}/V_m	$Q \times f$ (GHz)	τ_f (ppm/°C)
0	880	3.28	96.9	10.5±0.1	11.0 ± 0.1	12.0 ± 0.1	44.88	0.1872	74,700±500	–64.1±1.0
0.25	880	3.27	97.1	11.5±0.1	12.0 ± 0.1	11.5 ± 0.1	44.45	0.1856	38,300±500	–1.6±1.0
0.5	880	3.25	97.2	12.9±0.1	13.4 ± 0.1	11.4 ± 0.1	43.96	0.1840	24,700±500	+69.9±1.0
0.75	880	3.24	97.3	13.7 ±0.1	14.3 ± 0.1	10.8 ± 0.1	43.50	0.1832	20,100±500	+169.1±1.0
1	880	3.22	97.2	15.4 ±0.1	16.0 ± 0.1	10.5 ± 0.1	43.04	0.1816	15,400±500	+267.2±1.0

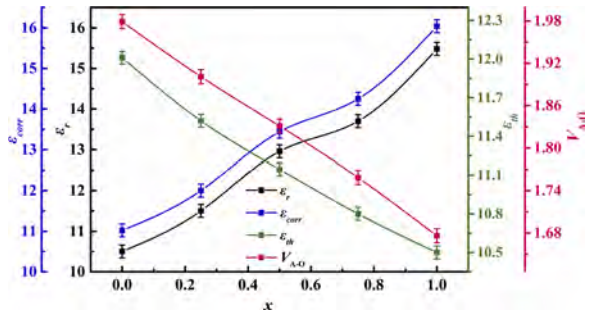

Fig. 5. The variation in ε_r, ε_{corr}, ε_{th} and $V_{A\text{-}O}$ of $Ca_{3-x}Mg_{1+x}LiV_3O_{12}$ ceramics.

measured ε_r to a slight extent, whereas ε_r and ε_{corr} increased with increased substitution of Mg^{2+} for Ca^{2+}. However, the trend of theoretical ε_{th} with x was rarely opposite to those of ε_r and ε_{corr}. With increased of x, α_{th}/V_m values decreased from 0.1872 ($x = 0$) to 0.1816 ($x = 1$), and then resulted in decreased ε_{th} from 12.0 ± 0.1 to 10.5 ± 0.1. Notably, the deviation between ε_{corr} and ε_{th} increased rapidly from –8.9 % to 34.5 %. These deviations can be explained by the existence of "compressed" cations and "rattling" cations, leading to low and high polarizabilities existing in the structure, which can be described by the bond valence of the A-site ($V_{A\text{-}O}$). Bond valence can be calculated by Formulas (5) and (6):

$$V_i = \sum_j V_{ij} \tag{5}$$

$$V_{ij} = \exp\left[\frac{R_{ij} - d_{ij}}{b}\right] \tag{6}$$

where, R_{ij} refers to the bond-valence parameter, d_{ij} denotes the length of a bond between atom i and j, and b is generally a constant equal to 0.37 Å [34]. The A-site bond length and bond valence in $Ca_{3-x}Mg_{1+x}LiV_3O_{12}$ ceramics are listed in Table S2. For $x = 0$, the mean bond valence of Ca^{2+} was calculated as 1.98, which was very near to the theoretical value of 2, indicating that $Ca_3MgLiV_3O_{12}$ was a stable garnet compound without "rattling" effect at the A-site. As the replacement of Mg^{2+} for Ca^{2+} increased, the bond valence of dodecahedral Ca^{2+} ranged from 1.979 to 2.030, which closely approached the theoretical value of 2. However, the bond valence of dodecahedral Mg^{2+} ranged from 0.950 to 0.968, which deviated largely from the theoretical value of 2, resulting in decreased $V_{A\text{-}O}$ from 1.98 to 1.68, and thus leading to decreased bond strength. These results suggested that the A-site occupation of the smaller Mg^{2+} cation may lead to relative instability of the garnet structure. Meanwhile, the decrease in $V_{A\text{-}O}$ enhanced the "rattling" effect and increased the dielectric polarizability of samples, followed by an increase in ε_r [35]. The similarly large deviation in ε_{corr} and ε_{th} were observed in garnet $Mg_3Y_2Ge_3O_{12}$ ceramics, and these deviations were ascribed to the presence of the "rattling" effect at the A-site [13]. Meanwhile, in AGe_4O_9 (A = Ba, Sr) ceramics, the higher measured permittivity than the theoretical permittivity was also due to the A-site rattling effect [15].

The variations of τ_f, τ_ε, and $V_{A\text{-}O}$ as a function of x for $Ca_{3-x}Mg_{1+x}LiV_3O_{12}$ ceramics are shown in Fig. 6. In general, τ_f is strongly correlated with the coefficient of thermal expansion (α_l) and the temperature coefficient of dielectric constant (τ_ε) [36]:

$$\tau_f = -\left(\frac{\tau_\varepsilon}{2} + \alpha_l\right) \tag{7}$$

For microwave dielectric ceramics, α_l is approximately 10 ppm/°C. Thus, τ_ε plays a key role in the magnitude of τ_f. The back-calculated τ_ε values 108.2 ppm/°C for $x = 0$ and –554.4 ppm/°C for $x = 1$ from the above equation were very close to the measured τ_ε values (86.9 ppm/°C

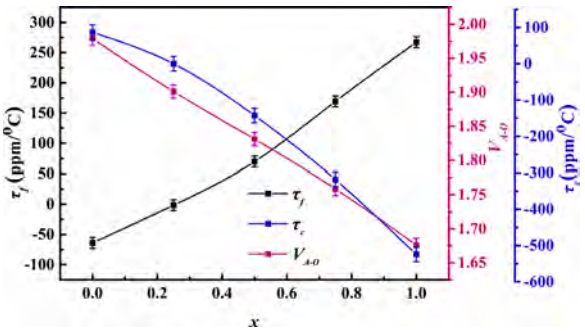

Fig. 6. The variation in τ_f, τ_ε and $V_{A\text{-}O}$ of $Ca_{3-x}Mg_{1+x}LiV_3O_{12}$ ceramics.

and –524.2 ppm/°C). Moreover, $V_{A\text{-}O}$ affected the τ_f of the samples. With increased x, the mean $V_{A\text{-}O}$ decreased from 1.98 to 1.68, showing that the rattling effect at the A-site of $Ca_{3-x}Mg_{1+x}LiV_3O_{12}$ increased and the energy required for the structural restoration decreased, resulting in a rapid increase in τ_f from –64.1 ± 1.0 ppm/°C to +267.2 ± 1.0 ppm/°C. Such a largely positive τ_f is very rare in low-permittivity microwave dielectric ceramics and has been reported only in our earlier work on $Mg_3Y_2Ge_3O_{12}$ [13].

Fig. 7 shows the $Q \times f$ values of $Ca_{3-x}Mg_{1+x}LiV_3O_{12}$ ceramics. With increased substitution of Mg^{2+} for Ca^{2+}, $Q \times f$ values decreased. For $Ca_{3-x}Mg_{1+x}LiV_3O_{12}$ ceramics, the relative densities of all ceramics were above 96 %, indicating that structural characteristics were important factors affecting $Q \times f$. Structural characteristics can be assessed by packing fraction, which is calculated as follows:

$$packing\ fraction(\%) = \frac{volume\ of\ packed\ ions}{volume\ of\ unit\ cell} \times Z \tag{7}$$

As the Mg^{2+} content increased, packing fraction and $Q \times f$ values decreased. With decreased packing fraction, lattice vibration increased and $Q \times f$ decreased [37]. Furthermore, based on the classical radiation theory, the variation in $Q \times f$ is associated with the FWHM value of the Raman active mode. Previous studies have shown that intrinsic loss is posed by non-harmonic vibration, and the connection between them can be illustrated by Formulas (8) and (9) [38]:

$$\tan\sigma = \frac{\gamma\omega_0}{\omega_T^2} \tag{8}$$

$$FWHM = \frac{\gamma\sqrt{\gamma^2 + 4\omega^2}}{2\omega_0} \tag{9}$$

where ω_0 is the central frequency of the optical mode, and ω_T is the angular frequency of the lattice vibration. The FWHM of the A_{1g} modes at around 829.7 cm^{-1} is shown in Fig. 7. The increase in FWHM corresponded to increased damping coefficient, leading decreased $Q \times f$ [39]. Furthermore, the bond valence of A-site cations affected the dielectric loss of the ceramics. As bond valence decreased, the damping constant of microwave signal increased because of the increase in non-harmonic interaction, resulting in increased dielectric loss and decreased $Q \times f$. For $Ca_{3-x}Mg_{1+x}LiV_3O_{12}$ ceramics, the mean $V_{A\text{-}O}$ gradually decreased with increased x, resulting in decreased $Q \times f$. The two different cations at the A-site probably caused the enhancement in anharmonic vibration, thereby further increasing the dielectric loss and decreasing the $Q \times f$ [40].

To meet the requirements of LTCC application, the chemical compatibility of $Ca_{2.75}Mg_{1.25}LiV_3O_{12}$ ceramic with near-zero τ_f between Ag powders was investigated. Fig. 8 shows that except for the diffraction peaks of $Ca_{2.75}Mg_{1.25}LiV_3O_{12}$ and Ag, no other peaks were found, indicating that no chemical reaction occurred between $Ca_{2.75}Mg_{1.25}LiV_3O_{12}$ ceramic and Ag. From the inset of Fig. 8, the grain boundary between $Ca_{2.75}Mg_{1.25}LiV_3O_{12}$ ceramics and Ag powders was clearly distinguished, exhibiting good chemical compatibility with Ag. Therefore, $Ca_{2.75}Mg_{1.25}LiV_3O_{12}$ ceramic could be considered as a potential material for LTCC applications with the advantages of low sintering temperature, excellent microwave performance, and good compatibility with Ag electrodes.

4. Conclusions

A series of garnet-structure microwave dielectric ceramics $Ca_{3-x}Mg_{1+x}LiV_3O_{12}$ (x = 0, 0.25, 0.5, 0.75, 1), was obtained by the conventional solid-state method. Their phase composition, microstructure, sintering behavior, crystal structure, and microwave dielectric properties were investigated in detail. Results showed that replacing Ca^{2+} with Mg^{2+} greatly affected the performance of the system. Based on XRD and Rietveld refinement results, all ceramics crystallized into a cubic garnet-structure with space group *Ia*-3*d* and had impurities. The lattice parameter and cell volume slightly decreased with increased Mg^{2+} replacing Ca^{2+}. Importantly, with increased substitution of Mg^{2+} for Ca^{2+}, the mean $V_{A\text{-}O}$ decreased from 1.98 to 1.68, exerting increased rattling effect. ε_r gradually increased from 10.5 ± 0.1 to 15.4 ± 0.1 with increased x, whereas the theoretical ε_{th} decreased gradually from 12.0 ± 0.1 to 10.5 ± 0.1. The large deviation between ε_{corr} and ε_{th} increased rapidly from –8.9 % to 34.5 %, which was ascribed to the existence of "compressed" and "rattling" cations leading to low and high polarizabilities, respectively. Moreover, the enhanced "rattling" effect caused τ_f to increase rapidly from –64.1 ± 1.0 ppm/°C to the large +267.2 ± 1.0 ppm/°C. $Q \times f$ values decreased rapidly from 74,700 ± 500 GHz to 15,370 ± 500 GHz with x, which was attributed to the decreased packing fraction, increased FWHM of the A_{1g} modes, and enhanced "rattling" effect. Additionally, $Ca_{2.75}Mg_{1.25}LiV_3O_{12}$ ceramics exhibited a good compatibility with Ag electrodes, making it good candidate for LTCC applications.

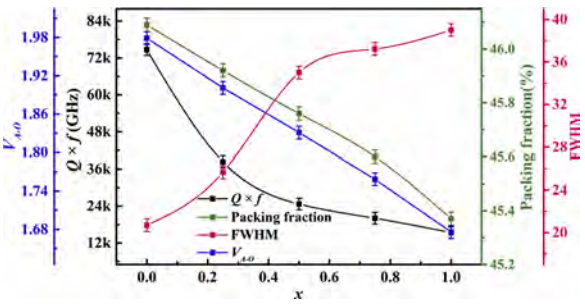

Fig. 7. The variation in $Q \times f$, packing fraction, FWHM and A-site bond valence of $Ca_{3-x}Mg_{1+x}LiV_3O_{12}$ ceramics.

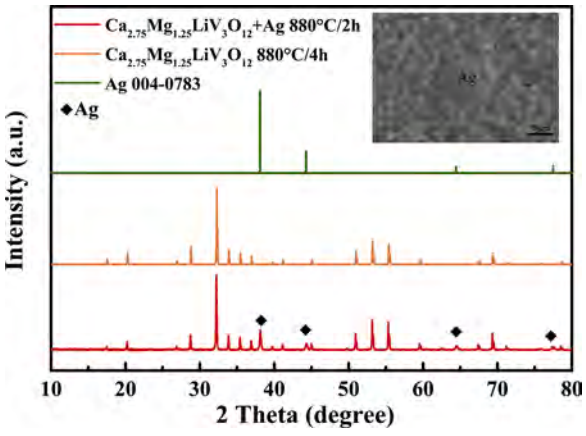

Fig. 8. XRD patterns and BSE images of $Ca_{2.75}Mg_{1.25}V_3LiO_{12}$ ceramics co-fired with 20 wt% Ag powders at 880 °C for 2 h.

Declaration of Competing Interest

The authors declare that they have no known competing financial interests or personal relationships that could have appeared to influence the work reported in this paper.

Acknowledgments

This work was supported by the Natural Science Foundation of China (Nos. 21761008 and 21965009), the Natural Science Foundation of Guangxi Zhuang Autonomous Region(Nos. 2018GXNSFAA138175 and AD20297035), and the Project funded by China Postdoctoral Science Foundation (2020M683628XB).

Appendix A. Supplementary data

Supplementary material related to this article can be found, in the online version, at doi:https://doi.org/10.1016/j.jeurceramsoc.2021.08.007.

References

[1] H.H. Guo, D. Zhou, L.X. Pang, Z.M. Qi, Microwave dielectric properties of low firing temperature stable scheelite structured (Ca,Bi)(Mo,V)O4 solid solution ceramics for LTCC applications, J. Eur. Ceramic. Soc. 39 (2019) 2365–2373.
[2] Z.Y. Zou, Z.H. Chen, X.K. Lan, W.Z. Lu, B. Ullah, X.H. Wang, W. Lei, Weak ferroelectricity and low-permittivity microwave dielectric properties of Ba2Zn(1+x) Si2O(7+x) ceramics, J. Eur. Ceram. Soc. 37 (2017) 3065–3071.
[3] Z.W. Zhang, L. Fang, H.C. Xiang, M.Y. Xu, Y. Tang, H. Jantunen, C.C. Li, Structural, infrared reflectivity spectra and microwave dielectric properties of the Li7Ti3O9F ceramic, Ceram. Int. 45 (2019) 10163–10169.
[4] D. Zhou, L.X. Pang, D.W. Wang, I.M. Reaney, BiVO4 based high k microwave dielectric materials: a review, J. Mater. Chem. C 6 (2018) 9290–9313.
[5] M. Sebastian, R. Ubic, H. Jantunen, Low-loss dielectric ceramic materials and their properties, Int. Mater. Rev. 60 (2015) 392–412.
[6] D. Zhou, J. Li, L.X. Pang, D.W. Wang, I.M. Reaney, Novel water insoluble (NaxAg2-x)MoO4($0 \leq x \leq 2$) microwave dielectric ceramics with spinel structure sintered at 410 degrees, J. Mater. Chem. C 5 (2017) 6086–6091.
[7] L. Fang, C.X. Su, H.F. Zhou, Z.H. Wei, H. Zhang, Novel Low-Firing Microwave Dielectric Ceramic LiCa3MgV3O12 with Low Dielectric Loss, J. Am. Ceram. Soc. 96 (2013) 688–690.
[8] C.X. Su, L. Fang, Z.H. Wei, X.J. Kuang, H. Zhang, LiCa3ZnV3O12: A novel low-firing, high Q microwave dielectric ceramic, Ceram. Int. 40 (2014) 5015–5018.
[9] J.Q. Chen, Y. Tang, H.C. Xiang, L. Fang, H. Porwal, C.C. Li, Microwave dielectric properties and infrared reflectivity spectra analysis of two novel low-firing AgCa2B2V3O12 (B = Mg, Zn) ceramics with garnet structure, J. Eur. Ceram. Soc. 38 (2018) 4670–4676.
[10] B. Li, H.S. Leng, W. Liu, Influence of the sintering process on microstructures and microwave properties of Ca5Ni2Mg2V6O24 ceramics, Mater. Chem. Phys. 253 (2020) 123371–123377.
[11] R. Madhuri, S. Ganesanpoti, Crystal structure, phonon modes, and bond characteristics of AgPb2B2V3O12 (B = Mg, Zn) microwave ceramics, J. Am. Ceram. Soc. 103 (2020) 3157–3167.
[12] H. Luo, W. Fang, L. Fang, W. Li, C. Li, Y. Tang, Microwave dielectric properties of novel glass-free low temperature firing ACa2Mg2V3O12 (A = Li, K) ceramics, Ceram. Int. 42 (2016) 10506–10510.
[13] Y. Tang, Z.W. Zhang, J. Li, M.Y. Xu, Y.F. Zhai, L. Duan, C.X. Su, L.J. Liu, Y.H. Sun, L. Fang, A3Y2Ge3O12 (A = Ca, Mg): Two novel microwave dielectric ceramics with contrasting τf and Q × f, J. Eur. Ceram. Soc. 40 (2020) 3989–3995.
[14] F.H. Li, Y. Tang, J. Li, W.S. Fang, L.Y. Ao, Y. Wang, X.G. Zhao, L. Fang, Effect of A-site cation on crystal structure and microwave dielectric properties of AGe4O9 (A = Ba, Sr) ceramics, J. Eur. Ceram. Soc. 41 (2021) 4153–4159.
[15] J.D. Dunitz, L.E. Orgel, Stereochemistry of Ionic Solids, Adv. Inorg. Chem. Radiochem. 2 (1960) 1–60.
[16] M.S. Fu, L. Ni, X.M. Chen, Abnormal variation of microwave dielectric properties in A/B site co-substituted (Ca1−0.3xLa0.2x)[(Mg1/3Ta2/3)1−xTix]O3 complex perovskite ceramics, J. Eur. Ceram. Soc. 33 (2013) 813–823.
[17] H.S. Park, K.H. Yoon, E.S. Kim, Effect of bond valence on microwave dielectric properties of complex perovskite ceramics, Mater. Chem. Phys. 79 (2003) 181–183.
[18] Y.S. Ch, K.H. Yoon, B.D. Lee, H.R. Lee, E.S. Kim, Understanding microwave dielectric properties of Pb-based complex perovskite ceramics via bond valence, Ceram. Int. 30 (2004) 2247–2250.
[19] R.D. Shannon, Dielectric polarizabilities of ions in oxides and fluorides, J. Appl. Phys. 73 (1993) 348–366.
[20] H. Takuya, A. Yusuke, K. Atsuya, U. Tadaharu, T. Kenji, S. Mineo, Bluish-White Luminescence in Rare-Earth-Free Vanadate Garnet Phosphors: Structural Characterization of LiCa3MV3O12 (M = Zn and Mg), Inorg. Chem. 57 (2018) 857–866.
[21] J.C. Zhou, X.T. Huang, J.H. You, B. Wang, H.D. Chen, Q.S. Wu, Synthesis, energy transfer and multicolor luminescent property of Eu3+-doped LiCa2Mg2V3O12 phosphors for warm white light-emitting diodes, Ceram. Int. 45 (2019) 13832–13837.
[22] J. Rodríguez-Carvajal, Recent advances in magnetic structure determination by neutron powder diffraction, Phys. B Condens. Matter. 192 (1993) 55–69.
[23] M.I. Mendelson, Average Grain Size in Polycrystalline Ceramics, J. Am. Ceram. Soc. 52 (1969) 443–446.
[24] B.W. Hakki, P.D. Coleman, A dielectric resonator method of measuring inductive capacities in the millimeter range, IRE Trans, Microw. Theory Tech. 8 (1960) 402–410.
[25] Q.L. Dai, R.Z. Zuo, Y.D. Xu, L.G. He, A novel temperature-stable Ba2-xCaxMgTi5O13 microwave dielectric ceramic, J. Eur. Ceram. Soc. 40 (2020) 376–380.
[26] D. Levy, J. Barbier, Normal and inverse garnets: Ca3Fe2Ge3O12, Ca3Y2Ge3O12 and Mg3Y2Ge3O12, Acta Crystallogr. Sect. C: Cryst. Struct. Commun. 55 (1999) 1611–1614.
[27] A. Bindhu, J.I. Naseemabeevi, S. Ganesanpotti, Distortion and energy transfer assisted tunability in garnet phosphors, Crit. Rec Solid. State 5 (2021) 1–44.
[28] A. Dutta, S.K. Singh, V.R.K. Murthy, P.K. Mukhopadhyay, T.P. Sinha, Crystal structure, Raman spectroscopy and microwave dielectric properties of xBa3MgNb2O9–(1-x)Ba2InNbO6 [x=0.4, 0.6, 0.8], Mater. Res. Bull. 100 (2018) 178–183.
[29] M. Rakhi, G. Subodh, Crystal structure and microwave dielectric properties of NaPb2B2V3O12 (B = Mg, Zn) ceramics, J. Eur. Ceram. Soc. 38 (2018) 4962–4966.
[30] W. Lei, W.Z. Lu, D. Liu, J.H. Zhu, Phase Evolution and Microwave Dielectric Properties of (1−x)ZnAl2O4−xMg2TiO4 Ceramics, J. Am. Ceram. Soc. 92 (2010) 105–109.
[31] H. Ogawa, A. Kana, S. Ishihara, Y. Higashida, Crystal structure of corundum type Mg4(Nb2-xTax)O9 microwave dielectric ceramics with low dielectric loss, J. Eur. Ceram. Soc. 23 (2003) 2485. –248.
[32] A.J. Bosman, E.E. Havinga, Temperature dependence of dielectric constants of cubic ionic compounds, Phys. Rev. 129 (1963) 1593–1600.
[33] S.H. Yoon, D.W. Kim, S.Y. Cho, K.S. Hong, Investigation of the relations between structure and microwave dielectric properties of divalent metal tungstate compounds, J. Eur. Ceram. Soc. 26 (2006) 2051–2054.
[34] N.E. Brese, M. OKeeffe, Bond-valence parameters for solids, Acta Crystallogr. 47 (1991) 192–197.
[35] M. Xiao, Q. Gu, Z. Zhou, P. Zhang, Study of the microwave dielectric properties of (La1-xSmx)NbO4(x=0-0.10) ceramics via bond valence and packing fraction, J. Am. Ceram. Soc. 100 (2017) 3952–3960.
[36] I.M. Reaney, D. Iddles, Microwave dielectric ceramics for resonators and filters in mobile phone networks, J. Am. Ceram. Soc. 89 (2006) 2063–2072.
[37] S.Y. Wang, J.D. Chen, Y.J. Zhang, Y.C. Zhang, Crystal structure and microwave dielectric properties of a new lowloss ceramic NiTiTa2O8, J. Alloys. Compd. 805 (2019) 852–858.
[38] R. Zurmühlen, J. Petzelt, S. Kamba, V.V. Valentin, E. Colla, Dielectric spectroscopy of Ba(B1/2B1/2)O3 complex perovskite ceramics: Correlations between ionic parameters and microwave dielectric properties. I. Infrared reflectivity study (1012-1014 Hz), Appl. Phys. 77 (1995) 5341–5350.
[39] C. Xing, J.Z. Li, H.L. Chen, H.Y. Qiao, J. Yang, H.L. Dong, H.Q. Sun, J. Wang, X. Q. Yin, Z.M. Yin, F. Shi, Phonon characteristics, crystal structure, and intrinsic properties of a Y(Mg1/2Sn1/2)O3 ceramic, RSC. ADV. 7 (2017) 35305–35310.
[40] S.K. Singh, V. Murthy, Crystal structure, Raman spectroscopy and microwave dielectric properties of layered-perovskite BaA2Ti3O10 (A= La, Nd and Sm) compounds, Mater. Chem. Phys. 160 (2015) 187–193.